ORIGINAL ARTICLE

Cryopreserved human skin allografts promote angiogenesis and dermal regeneration in a murine model

Dominic Henn[1,2] | Kellen Chen[1] | Zeshaan N. Maan[1] | Autumn H. Greco[1] | Sylvia E. Moortgat Illouz[1] | Clark A. Bonham[1] | Janos A. Barrera[1] | Artem A. Trotsyuk[1] | Jagannath Padmanabhan[1] | Arash Momeni[1] | Derrick C. Wan[1] | Dung Nguyen[1] | Michael Januszyk[1] | Geoffrey C. Gurtner[1]

[1]Hagey Laboratory for Pediatric and Regenerative Medicine, Division of Plastic and Reconstructive Surgery, Department of Surgery, Stanford University, Stanford, California

[2]Department of Hand, Plastic, and Reconstructive Surgery, BG Trauma Center Ludwigshafen, Ruprecht-Karls-University of Heidelberg, Heidelberg, Germany

Correspondence
Geoffrey C. Gurtner, MD, FACS, Johnson and Johnson Distinguished Professor of Surgery, Professor (by courtesy) of Bioengineering and Materials Science, Inaugural Vice Chairman of Surgery for Innovation, Former, Inaugural Vice Chairman of Surgery for Research (2009-2019), Stanford University School of Medicine, 257 Campus Drive West, GK-201, Stanford, CA.
Email: ggurtner@stanford.edu

Funding information
Stanford University

Abstract

Cryopreserved human skin allografts (CHSAs) are used for the coverage of major burns when donor sites for autografts are insufficiently available and have clinically shown beneficial effects on chronic non-healing wounds. However, the biologic mechanisms behind the regenerative properties of CHSA remain elusive. Furthermore, the impact of cryopreservation on the immunogenicity of CHSA has not been thoroughly investigated and raised concerns with regard to their clinical application. To investigate the importance and fate of living cells, we compared cryopreserved CHSA with human acellular dermal matrix (ADM) grafts in which living cells had been removed by chemical processing. Both grafts were subcutaneously implanted into C57BL/6 mice and explanted after 1, 3, 7, and 28 days (n = 5 per group). A sham surgery where no graft was implanted served as a control. Transmission electron microscopy (TEM) and flow cytometry were used to characterise the ultrastructure and cells within CHSA before implantation. Immunofluorescent staining of tissue sections was used to determine the immune reaction against the implanted grafts, the rate of apoptotic cells, and vascularisation as well as collagen content of the overlaying murine dermis. Digital quantification of collagen fibre alignment on tissue sections was used to quantify the degree of fibrosis within the murine dermis. A substantial population of live human cells with intact organelles was identified in CHSA prior to implantation. Subcutaneous pockets with implanted xenografts or ADMs healed without clinically apparent rejection and with a similar cellular immune response. CHSA implantation largely preserved the cellularity of the overlying murine dermis, whereas ADM was associated with a significantly higher rate of cellular apoptosis, identified by cleaved caspase-3 staining, and a stronger dendritic cell infiltration of the murine dermis. CHSA was found to induce a local angiogenic response,

leading to significantly more vascularisation of the murine dermis compared with ADM and sham surgery on day 7. By day 28, aggregate collagen-1 content within the murine dermis was greater following CHSA implantation compared with ADM. Collagen fibre alignment of the murine dermis, correlating with the degree of fibrosis, was significantly greater in the ADM group, whereas CHSA maintained the characteristic basket weave pattern of the native murine dermis. Our data indicate that CHSAs promote angiogenesis and collagen-1 production without eliciting a significant fibrotic response in a xenograft model. These findings may provide insight into the beneficial effects clinically observed after treatment of chronic wounds and burns with CHSA.

KEYWORDS

allograft, angiogenesis, fibrosis, split thickness skin graft, wound healing

1 | INTRODUCTION

For more than 50 years, transplantation of human skin allografts has been the gold standard for the temporary coverage of major burns when donor sites for autologous skin grafts are insufficiently available.[1] Beyond the initial goal of temporary wound coverage to decrease fluid loss and prevent infections, skin allografts have also shown beneficial effects in the treatment of major burns by preparing the wound bed for future autograft applications. Skin allografts have been shown to improve wound regeneration not only in burns[2-4] but also in chronic venous as well as diabetic lower leg ulcers, leading to higher healing rates compared with bioengineered skin substitutes.[5-8] The most commonly used methods for preservation of human skin allografts in tissue banks are dehydration using highly concentrated glycerol or cryopreservation (-20 to $-196°C$). Cryopreservation has been suggested to be the preferred method of skin graft preservation, as it better preserves the physicochemical properties and viability of fresh human skin.[9-11] However, limited data exist on the impact of cryopreservation on the immunogenicity of skin allografts and concerns about immunological sensitisation after skin allograft transplantation have been raised.[12] Due to their incompatibility with the host, the cellular elements of skin allografts are rejected, though dermal components can persist and become incorporated into the healing host dermis.[3] The biologic mechanisms underlying this integration, which have been clinically demonstrated after skin allotransplantation, remain incompletely understood. In order to characterise the impact of live cells within CHSA on the host immune response, we developed a xenograft model by subcutaneous transplantation of CHSA containing live cells or decellularised human

Key Messages

- the biologic mechanisms behind the regenerative properties of cryopreserved human skin allografts (CHSAs) on wound healing remain elusive and the impact of cryopreservation on the immunogenicity of CHSA has not been thoroughly investigated
- CHSAs and acellular dermal matrix (ADM) grafts were subcutaneously implanted into immunocompetent mice and explanted after 1, 3, 7, and 28 days. Transmission electron microscopy, flow cytometry, immunofluorescent staining of tissue sections, and digital quantification of collagen fiber alignment were used to characterise living cells in CHSA and to determine the immune response against the grafts as well as the rate of apoptotic cells, vascularisation, and collagen content and the architecture of the overlaying murine dermis
- CHSA was found to induce a local angiogenic response, leading to significantly more vascularisation of the murine dermis
- collagen fiber alignment of the murine dermis, correlating with the degree of fibrosis, was significantly greater after ADM implantation, whereas CHSA maintained the characteristic basket weave pattern of the native murine dermis

acellular dermal matrix (ADM) into immunocompetent mice. Our subcutaneous implantation model also allowed us to assess the impact of CHSA on murine dermal integrity over time.

2 | METHODS

2.1 | Subcutaneous implantation of CHSA and ADM

All experiments were performed in accordance with Stanford University Institutional Animal Care and Use Committees and have been approved by the Administrative Panel on Laboratory Animal Care at Stanford University (APLAC). Subcutaneous pockets were created via 1 cm incision and sharp dissection above the muscle fascia on the dorsum of C57BL/6J (wild-type) mice (Jackson Laboratory, Bar Harbor, ME) (n = 5 per group). CHSA (TheraSkin, Misonix, Inc, Farmingdale, NY) were thawed and grafts of 1×1 cm were implanted into the subcutaneous pockets. Implantation of ADM grafts (AlloDerm, Allergan, Dublin, Ireland) or sham pockets without graft implantation served as controls. Incisions were closed with 6-0 nylon sutures (Ethilon, Ethicon, Somerville, New Jersey). The grafts and overlaying murine skin were explanted after 1, 3, 7, and 28 days. The subcutaneous implantation model allowed us to directly investigate the impact of the implanted grafts on dermal integrity, collagen architecture, and cellular composition of the overlying murine dermis over time.

2.2 | Flow cytometry

For flow cytometric analysis, CHSA were thawed, then micro-dissected, and incubated in serum-free Dulbecco's Modified Eagle Medium (DMEM) with 240 U of collagenase IV/mL for 1 hour at 37°C in a rotating oven. Digested tissue was filtered, centrifuged, and stained with $4',6$-diamidino-2-phenylindole (DAPI) (Biolegend, San Diego, California). Cells were analysed on a BD FACS Aria (Becton Dickinson, San Jose, California) and data were analysed using FlowJo (Becton Dickinson, San Jose, California).

2.3 | Transmission electron microscopy

Sections were mounted on slides and fixed in Karnovsky's fixative (2% glutaraldehyde and 4% formaldehyde in 0.1 M sodium cacodylate pH 7.4 for 1 hour. The sections were post-fixed in cold 1% osmium tetroxide in water and allowed to warm for 2 hours in a hood, then washed three times with ultrafiltered water. Subsequently, sections were *en bloc* stained in 1% uranyl acetate at room temperature for 2 hours. Samples were dehydrated in serial ethanol washes for 10 minutes at room temperature and then washed in propylene oxide (PO) for 10 minutes. Samples were infiltrated with EMbed-812 resin mixed at 1:1 and 2:1 with PO for 2 hours each. Furthermore, the

samples were placed into EMbed-812 for 2 hours, placed into flat moulds with fresh resin, and then incubated in an oven at 65°C overnight. Sections of 90 nm were picked up on formvar/Carbon coated Cu grids, stained for 40 seconds in 3.5% uranyl acetate in 50% acetone, followed by staining in Sato's Lead for 2 minutes. Samples were analysed in the JEM-1400 120 kV transmission electron microscope (TEM; JEOL, Peabody, Massachusetts) and photos were taken using an Orius 2 k × 4 k digital camera (Gatan, Pleasanton, California).

2.4 | Histologic analysis

Explanted tissue was fixed in 4% paraformaldehyde (PFA) in phosphate-buffered saline (PBS) for 24 hours. For haematoxylin and eosin (H&E) and picrosirius red (PSR) staining, tissue was dehydrated in a graded ethanol series and embedded into paraffin. Tissue sections were deparaffinised and rehydrated through graded ethanol series. H&E staining and PSR staining were performed according to standard protocols.

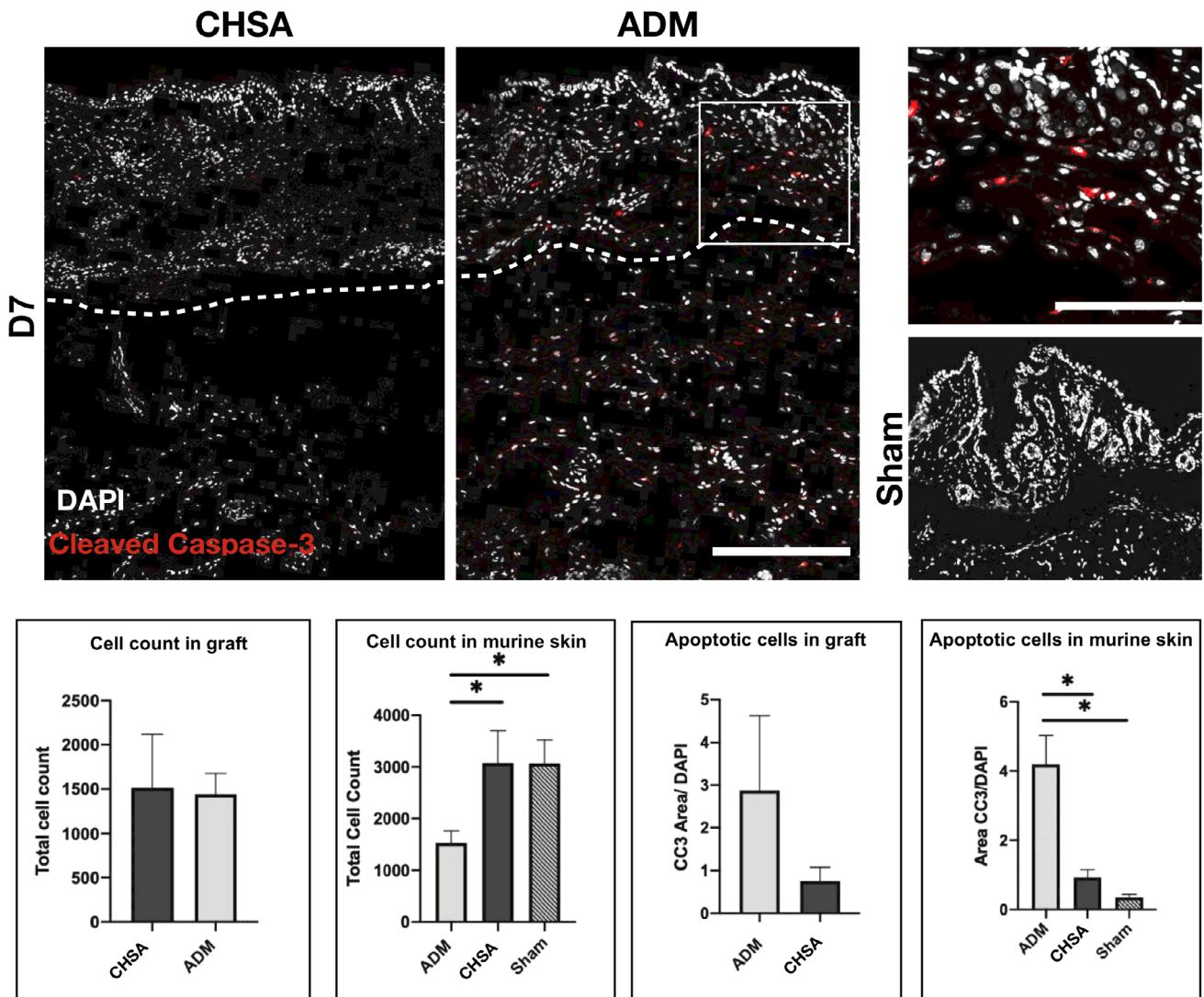### 2.5 | Immunofluorescent staining and confocal laser scanning microscopy

After fixation, tissue was dehydrated in 30% sucrose in 1X PBS for at least 48 hours at 4°C. Tissue was then incubated in optimal cutting temperature compound (O.C.T., TissueTek, Sakura Finetek, Torrance, California) for 24 hours at 4°C and then cryoembedded in tissue moulds on dry ice. Frozen sections were performed at 7 μm thickness on a cryostat. Antigen retrieval was performed using 0.01 M sodium citrate buffer in PBS (Abcam, Cambridge, MA), followed by blocking for 2 hours in 5% goat serum (Invitrogen, Waltham, Massachusetts,) in PBS. Sections were then incubated in anti-CD11c antibody (ab33483; Abcam, Cambridge, Massachusetts,), anti-myeloperoxidase antibody (PA5-16672, ThermoFisher, Waltham, Massachusetts,), anti-CD31 antibody (ab28364; Abcam) or anti-mouse collagen-1 antibody (AB765P; Millipore Sigma) over night at 4°C, followed by secondary antibody staining for 1 hour at room temperature. Slides were stained with DAPI for cell nuclei and mounted with cover slips.

2.6 | Automatic quantification of immunofluorescent staining and collagen fibre alignment

Immunofluorescent staining was quantified using a code written in MATLAB adapted from previous image
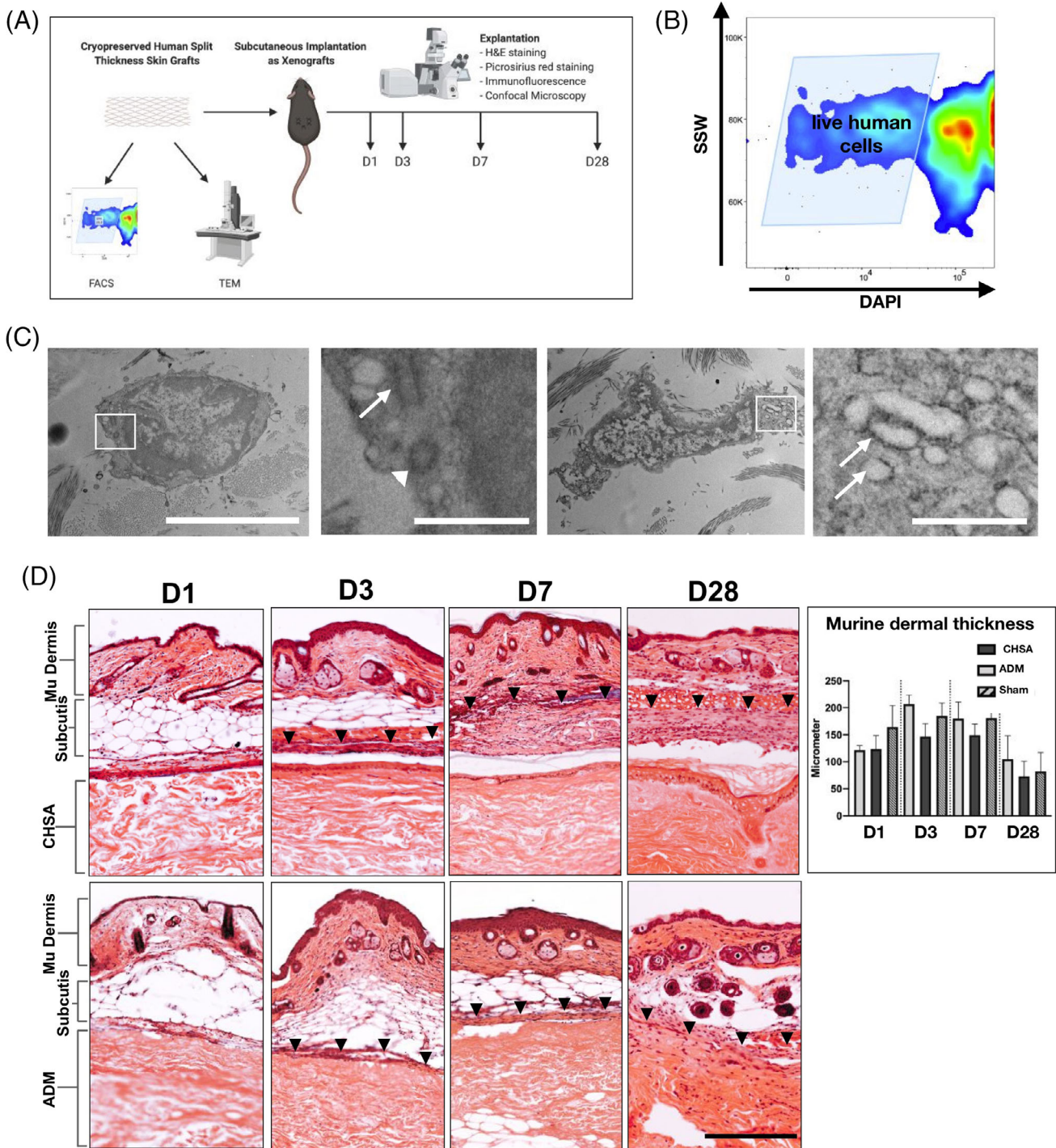
FIGURE 1 A, Schematic of the experiments performed to establish the xenograft model (created with biorender.com). Cryopreserved human skin allografts (CHSA) were analysed by flow cytometry (FACS) and transmission electron microscopy (TEM). in vivo implantation of CHSA and an acellular dermal matrix (ADM) was performed subcutaneously into C57BL6/J mice. Explantation was performed on days 1, 3, 7, and 28 for H&E and picrosirius red staining as well as immunofluorescent staining and confocal microscopy. B, Single cell suspensions derived from thawed CHSA were subjected to FACS, showing numerous live (DAPI-negative) cells. SSW, side scatter width. C, TEM revealed live cells with intact cell and nuclear membranes and functional organelles such as centrioles (second panel: arrow pointing to longitudinal section, arrowhead pointing to cross section) and rough endoplasmatic reticulum (fourth panel, arrows). White squares indicate the areas of the magnified images. Scale bars: 5 μm in overviews and 1 μm in magnified images. D, H&E images of explanted xenografts with overlaying murine (mu) subcutis and skin on days (d) 1, 3, 7, and 28. Arrowheads indicate the upper border of the fibrous capsule forming around the xenografts. Scale bar: 200 μm. H&E, haematoxylin and eosin
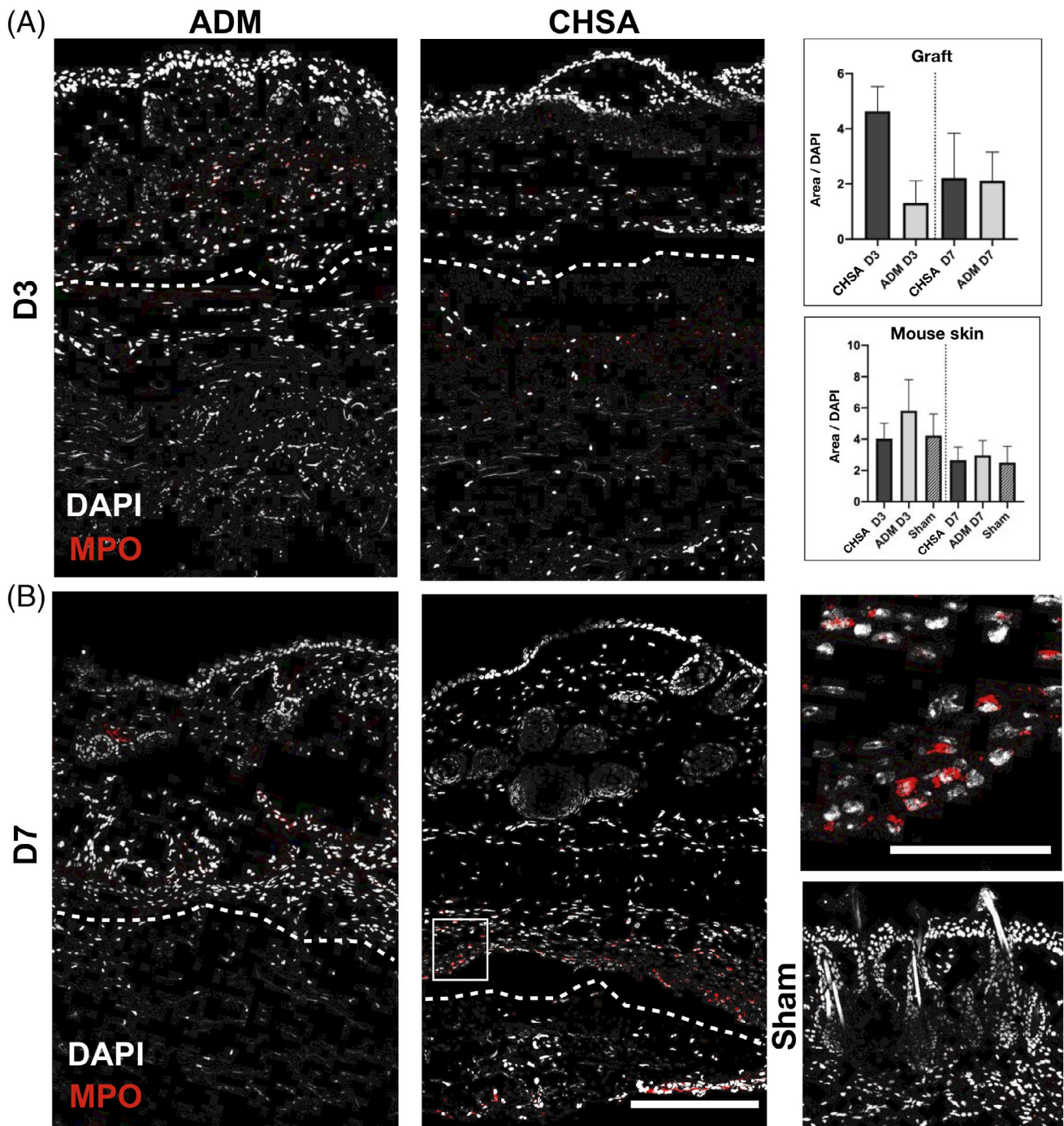
FIGURE 2 Immunofluorescent staining for cleaved caspase-3 (CC3) indicating apoptotic cells after implantation of cryopreserved human skin allografts (CHSA), acellular dermal matrix (ADM), or sham surgeries. White box indicating the area of the magnified image on the right. Dotted lines indicate the interface between murine dermis and xenografts. The white square indicates the area of the magnified image. Scale bar: 200 μm in overview and 100 μm in magnified image.*P < .05

analysis studies by one of the authors (K.C.).[13] Analysis of fibre alignment of the murine skin above ADM and CHSA was performed on polarised PSR images of 20× magnification using the custom software MatFiber. Fomovsky et al adapted this intensity-gradient-detection algorithm for MATLAB (Mathworks, Santa Clara, California),[14] and it has previously been used by the authors to analyse the alignment of collagen fibres and stress fibres.[13] We used this algorithm to analyse the angle of alignment and strength of alignment (mean vector length [MVL]) of subregions of 50 pixels in areas across the image with a threshold of 22 000. The MVL ranges from values of 0 (representing completely random alignment) to 1 (representing completely aligned fibres).

We used the MVL and mean angle (MA) of each image to then calculate an overall strength of alignment for the collagen fibres as mentioned previously.[14] Furthermore, collagen fibre quantification was performed using CT-FIRE, an open-source software package for automatic segmentation and quantification of individual collagen fibres (http://loci.wisc.edu/software/ctfire).[15]

Statistical analysis was performed in Prism8 (GraphPad, San Diego, California) using Student's t test or one-way analysis of variance (ANOVA) with Tukey's multiple comparisons test. The Rayleigh test was used to assess the circular distribution of the calculated vectors of alignment. Data are presented as means ± SEM. P values of <.05 were considered statistically significant.
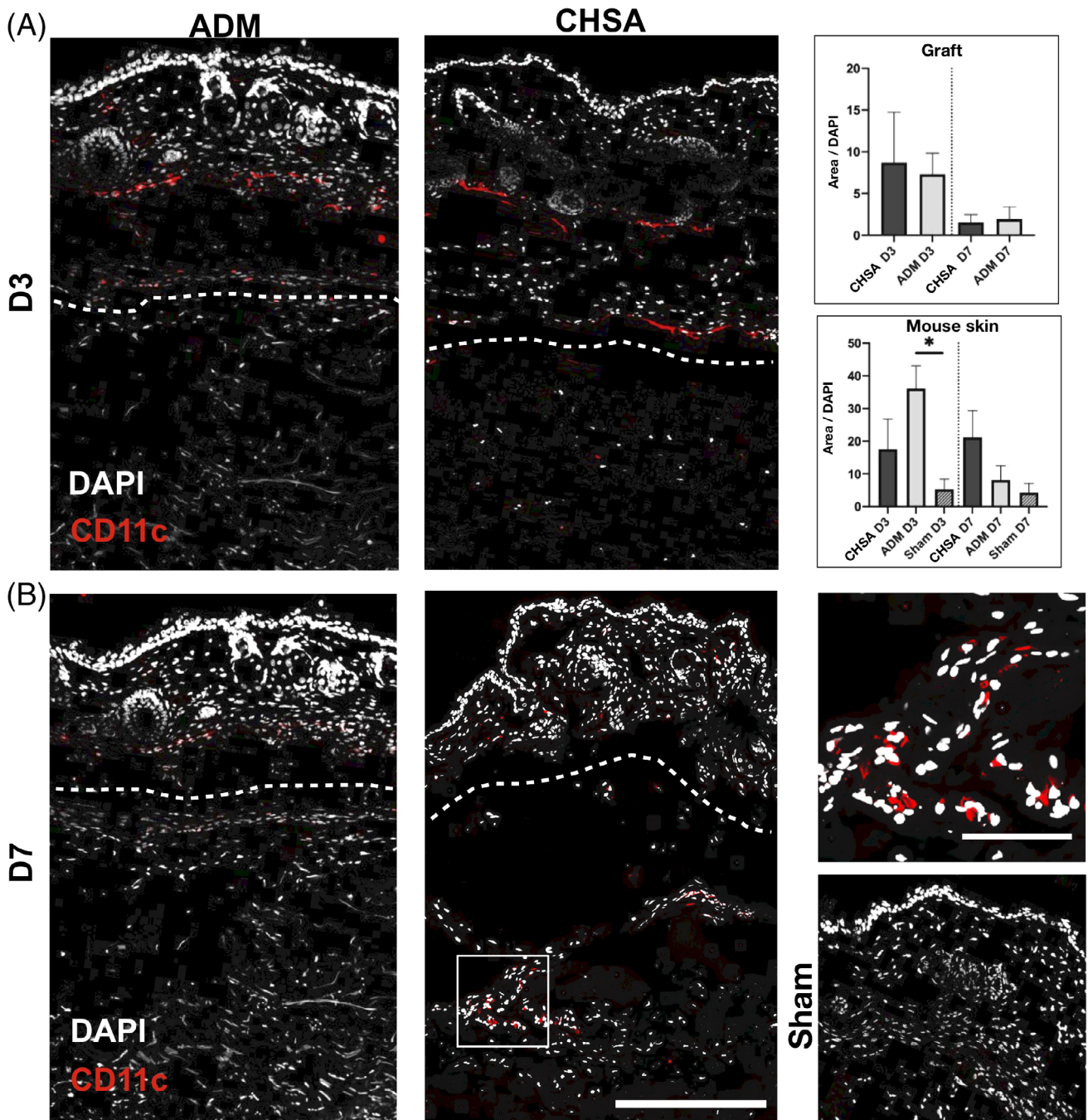
FIGURE 3 Immunofluorescent staining for myeloperoxidase (MPO) indicating neutrophilic granulocytes after implantation of cryopreserved human skin allografts (CHSA), acellular dermal matrix (ADM), or sham surgeries. Dotted lines indicate the interface between murine dermis and xenografts. The white square indicates the area of the magnified image. Scale bar: 200 μm in overview and 50 μm in magnified image.*$P < .05$

3 | RESULTS

3.1 | Human split thickness skin grafts exhibit live cells after cryopreservation and thawing

To identify the rate of live cells following cryopreservation, thawed CHSA were examined by FACS and TEM (Figure 1A). FACS analysis identified DAPI-negative (live) cells within the grafts (Figure 1B). TEM revealed cells with intact membranes and nuclei as well as functional organelles such as centrioles and rough endoplasmic reticulum, demonstrating active protein synthesis (Figure 1C).
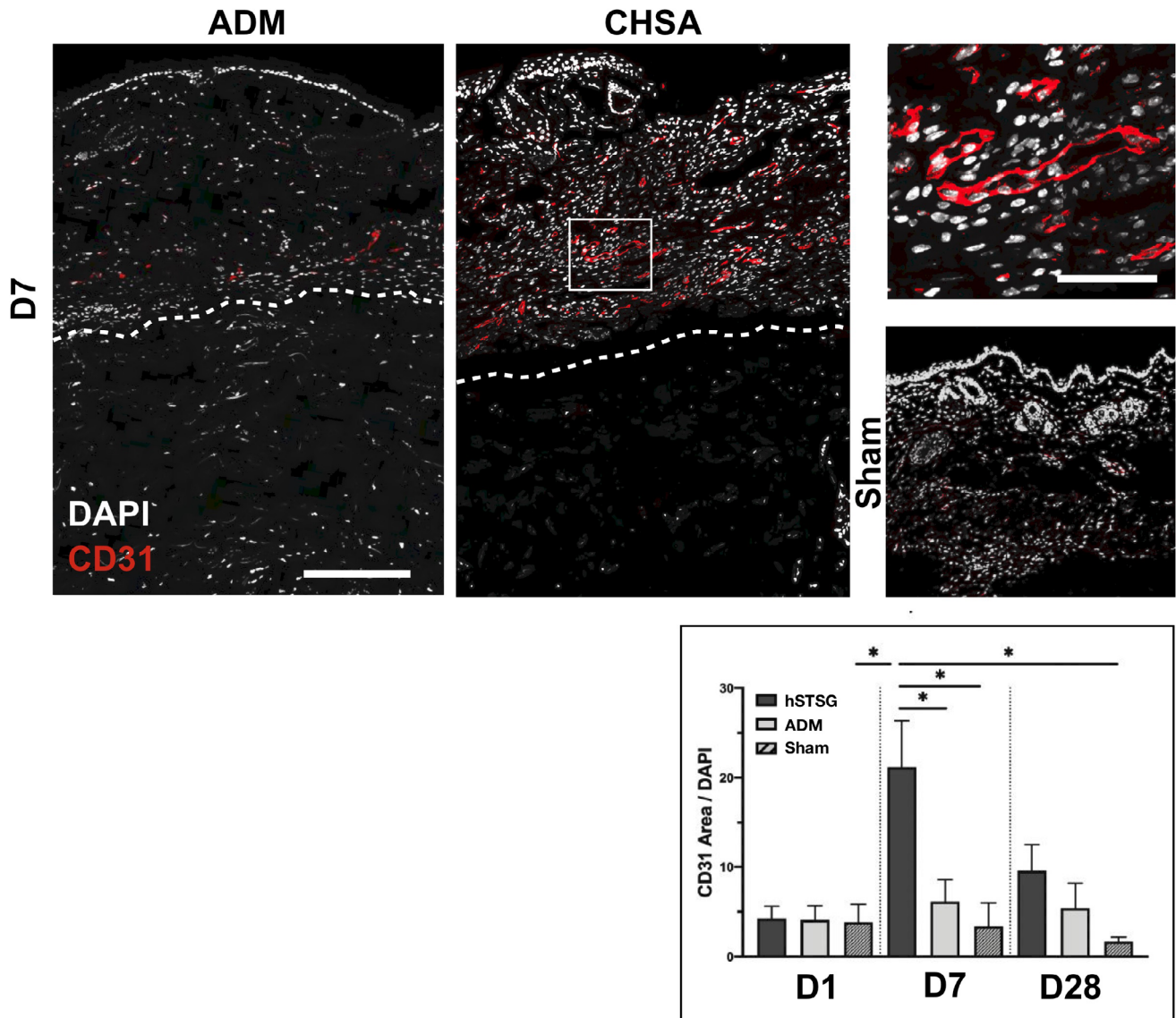
FIGURE 4 Immunofluorescent staining for CD11c indicating dendritic cells after implantation of cryopreserved human skin allografts (CHSA), acellular dermal matrix (ADM), or sham surgeries. Dotted lines indicate the interface between murine dermis and xenografts. The white square indicates the area of the magnified image. Scale bar: 200 μm in overview and 50 μm in magnified image.*$P < .05$

3.2 | Implantation of human xenografts preserves murine dermal integrity

All mice survived until the final timepoint of graft explantation at day 28. Healing of the skin incisions created for subcutaneous graft implantation occurred without any wound complications or macroscopically visible signs of inflammation within the overlying murine dermis, thus no clinically overt signs of graft rejection were observed. Xenograft implantation preserved murine dermal integrity, with intact hair follicles present through day 28 after graft implantation, and no significant differences in dermal thickness were observed over time. Fibrous capsule formation was stronger around CHSA compared with ADM (Figure 1D).

FIGURE 5 Immunofluorescent staining for CD31 indicating blood vessels in the murine dermis after implantation of cryopreserved human skin allografts (CHSA), acellular dermal matrix (ADM) implantation or sham surgeries. Dotted lines indicate the interface between murine dermis and xenografts. The white square indicates the area of the magnified image. Scale bar: 200 μm in overview and 50 μm in magnified image.*$P < 0.05$

## 3.3 | CHSA implantation is associated with less apoptosis of native murine dermis than ADM

Apoptotic cells were identified by immunofluorescent staining of cryoembedded tissue sections for cleaved caspase-3 and visualised by confocal microscopy. Overall, the cell count of the murine dermis was significantly higher after CHSA implantation and sham surgery compared with ADM implantation (Figure 2). Furthermore, ADM implantation showed a significantly higher rate of apoptotic, cleaved caspase-3-positive cells compared with CHSA and sham. Within the grafts, cellular infiltration was comparable between CHSA and ADM; however,

there was a trend towards a higher rate of apoptosis within ADM (Figure 2).

3.4 | CHSA do not elicit a stronger immune response than ADM

The acute and intermediate immune responses against the grafts were characterised by immunofluorescent staining against myeloperoxidase, an enzyme abundantly expressed in neutrophilic granulocytes, which catalyses the formation of reactive oxygen species,[16] as well as CD11c (integrin alpha X), an integrin found in high levels on most dendritic cell (DC) populations,[17] which
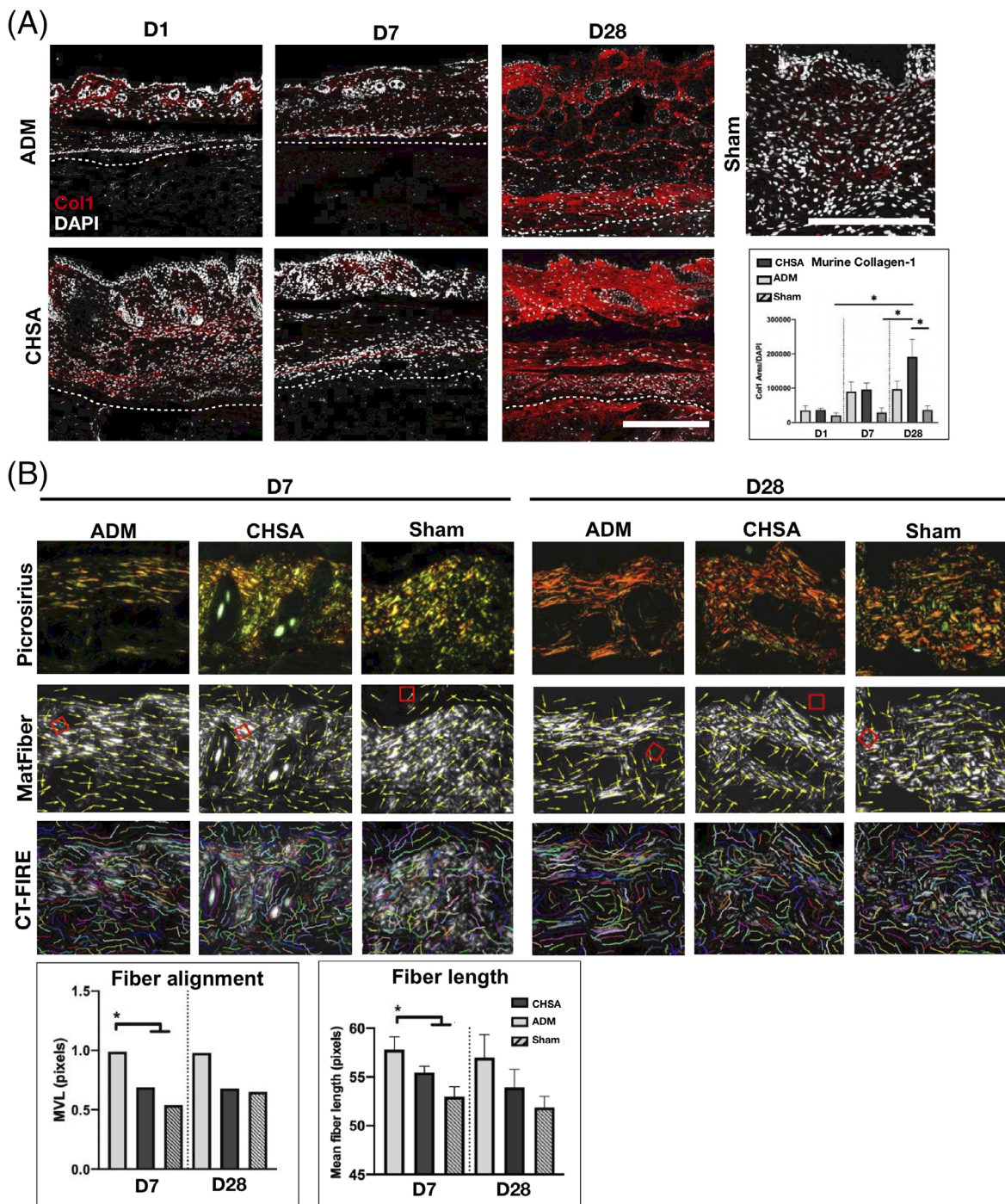
FIGURE 6 A, Immunofluorescent staining for murine collagen-1 after explantation of cryopreserved human skin allografts (CHSA) or acellular dermal matrix (ADM) on days 1, 7, and 28 after implantation and sham surgeries (postoperative day 7). Scale bar: 200 μm. B, Polarised images of picrosirius red-stained tissue sections and analysis of collagen fibre length (CT-FIRE) and alignment (MatFiber). *$P < .05$ compared with CHSA and sham calculated by Raleigh's test (fibre alignment) and one-way ANOVA (fibre length). MVL, mean vector length

are the main cell type to initiate adoptive alloimmunity.[18] Infiltration of the grafts by neutrophilic granulocytes trended to be higher in CHSA compared with ADM at day 3, however, without statistical significance ($P = .11$). No differences were seen after 7 days of implantation. Within the murine dermis, an overall stronger infiltration of granulocytes was seen on day 3 compared with day 7; however, neither graft induced stronger granulocyte infiltration than that associated with the creation of a sham pocket (Figure 3).

DCs were more abundant within both grafts on day 3 compared with day 7, though without statistical significance. ADM implantation induced a stronger DC

infiltration of the overlaying murine dermis compared with the sham pocket ($P < .05$), which also trended to be stronger than in CHSA. On day 7, there was a trend towards higher DC infiltration of the murine dermis in CHSA compared with ADM and sham (Figure 4).

3.5 | CHSA induce dermal angiogenesis

Vascularisation of the murine dermis was assessed by staining for CD31 (platelet endothelial cell adhesion molecule, PECAM-1) and was significantly greater on day 7 following CHSA implantation compared with ADM implantation or sham surgery, suggesting that CHSA promote angiogenic activity. No statistically significant differences in dermal vascularisation were found between the groups at baseline (day 1) and day 28 (Figure 5).

3.6 | CHSA implantation promotes collagen-1 production within the murine dermis without disrupting tissue ultrastructure

To assess the impact of CHSA and ADM on the murine dermal architecture and integrity within our xenograft model, we performed immunofluorescent staining for murine collagen-1 as well as PSR staining of tissue sections.

Collagen-1 content of the murine dermis increased in response to implantation of both xenografts and was significantly higher at day 28 in the CHSA group compared with sham operations ($P < .05$). A trend towards higher murine dermal collagen-1 content was also seen in CHSA compared with ADM (Figure 6A). To compare the degree of resulting fibrosis after xenograft implantation, we quantified collagen fibre length and alignment in polarised PSR images using automated software algorithms (MatFiber and CT-FIRE). A significantly higher fibre length and alignment within the murine dermis was found following ADM implantation on day 7, with the same trends still present through day 28, although statistically not significant, presumably due to the low sample size. This highly aligned collagen fibre pattern is more consistent with fibrosis of the wound bed. Conversely, CHSA implantation and sham surgeries preserved the characteristic basket weave appearance of the healthy murine dermis with shorter fibre lengths and lower alignment (Figure 6B).

4 | DISCUSSION

The beneficial effects of human skin allograft transplantation have been known for decades, particularly in the treatment of major burn injuries. Skin allografts have been shown to accelerate the healing of burn wounds and more also recently of chronic wounds.[7,19] As an immunogenic organ, allo- or xenografted skin by nature induces an immune response, ultimately leading to fibrotic encapsulation and rejection by the host.[20] Murine xenograft models have been widely used for the investigation of fibrotic conditions[21-23]; however, how the immune response to foreign grafts is linked to their clinically observed beneficial effects on wound healing has never been thoroughly investigated at the cellular or molecular levels.

To investigate the mechanisms underlying the regenerative effects of allogenic human skin grafts, as well as the role of live human cells within these grafts, we developed a xenograft model for CHSA and human ADM implantation into immunocompetent mice.

We found that the implantation of 1×1 cm large human xenografts with or without live cells was tolerated well by immunocompetent mice and did not induce wound complications or extrusion of the grafts through day 28.

Although cellular infiltration into the grafts was comparable between the groups, a reduced cell count within the murine dermis was found after ADM implantation. In line with these findings, staining for cleaved caspase-3 showed a higher rate of cellular apoptosis within the murine dermis after ADM compared with CHSA implantation, indicating a protective effect of CHSA on dermal integrity after injury. Previous studies have shown that soluble cytotoxic compounds from the decellularisation process of some types of ADM induce apoptosis in vitro and inflammation after subcutaneous implantation into mice,[24] which may be the cause of the increased cellular apoptosis found after ADM implantation in our study. The aseptic processing of AlloDerm includes a treatment with mild non-denaturing detergents to remove epidermal and dermal cells while the collagen matrix is preserved.[25] Remnants of such detergents within AlloDerm, which might locally be released after implantation, might be the reason for local cytotoxic effects and the increased cleavage of caspase-3 observed in this study. Clinical studies that have compared the use of aseptically processed and sterilised ADMs for breast reconstruction have yielded mixed results with regard to postoperative complication rates, and further research is required to define the impact of ADM processing techniques on the local tissue microenvironment.[25] For human MSCs, it has been shown that they reduce the cleavage of caspase-3 after xenotransplantation into the kidney capsule of immunocompetent mice,[26] which indicates similar effects of different xenotransplanted human cells in mouse models.

DCs are the main cell type mediating early immune recognition and rejection of allo- and xenogenic skin grafts. They present donor antigens on MHC molecules and elicit an adaptive immune response, secreting cytokines and acute-phase proteins.[27] A stronger infiltration of the murine dermis by DCs was found following implantation of ADM when compared with CHSA on day 3, indicating that live cells within CHSA do not trigger a stronger DC-mediated immune response compared with decellularised grafts. Neutrophilic granulocytes showed a trend towards a higher infiltration after CHSA implantation on day 3. However, neutrophilic infiltrates are not considered specific to the pathogenesis of skin graft rejection and rather represent a generic acute inflammatory response.[28]

CHSA transplantation induced angiogenesis and resulted in a significantly stronger vascularisation of the murine dermis on day 7 after graft implantation compared with ADM and sham surgeries. Previous studies have shown that the process of graft rejection is characterised by a hypoxic microenvironment leading to leukocyte infiltration, which secrete pro-angiogenic cytokines such as vascular endothelial growth factor.[29] Since it is well established that angiogenesis is critical for physiological wound healing,[30] the process of leukocyte-induced angiogenesis in response to CHSA transplantation might be the underlying mechanism behind the regenerative properties of CHSAs on wounds.

Collagen-1 content within the murine dermis increased by day 28 in response to ADM and CHSA implantation. CHSA transplantation induced a significantly higher collagen-1 expression compared with sham surgeries and a trend toward higher collagen-1 expression compared with ADM grafts. Although the production of collagen-1 by fibroblasts is an essential component of wound healing, collagen-1 accumulation is also a hallmark of fibrosis throughout different organ systems.[30] In order to characterise collagen architecture within the murine dermis after xenograft implantation, we analysed collagen fibre alignment within PSR-stained tissue sections, which has been shown to strongly correlate with the degree of fibrosis across different organ systems.[31] We found a significantly higher fibre alignment after ADM implantation compared with CHSA and sham surgery at post-implantation day 7. These findings indicate that the cellular response to CHSA might elicit a remodelling process of the dermis leading to a less fibrotic collagen fibre alignment, which preserves the physiologic basket weave appearance of the dermis. Our data might provide a biologic explanation for the improved healing rates of chronic wounds treated with CHSA compared with standard of care alone, which were demonstrated in large retrospective matched-cohort studies.[7,31]

Limitations of our study are related to the fact that the murine host response to CHSA may be different from the immune response to allografts in human patients. However, using a mouse xenograft model allowed us to investigate the response to CHSA and their impact on dermal integrity over time. Further limitations of our study are differences in the anatomy and physiology of the murine dermis compared with humans. Thus, studies using porcine models that resemble human skin more closely might yield valuable insights into the impact of skin allografts on dermal regeneration.[32] How living human cells within CHSA and different populations of host cells attracted in response to CHSA implantation impact dermal regeneration and angiogenesis on the molecular and cellular level has to be investigated in future studies. This will allow for a more in-depth understanding of the cellular mechanisms involved in the response to allograft tissues and how this relates to angiogenesis and extracellular matrix remodelling.

5 | CONCLUSIONS

Our data indicate that the implantation of CHSA induces murine dermal angiogenesis and regeneration, leading to an increased collagen-1 production with a lower degree of dermal fibrosis compared with human decellularised dermal grafts. Although a comparable immune response was observed after CHSA and ADM implantation, ADM induced a higher rate of cellular apoptosis within the murine dermis, which might be related to the decellularisation process during ADM fabrication. The beneficial impact of CHSA implantation on murine dermal regeneration in our xenograft model might be the underlying cause of the clinically observed regenerative effects after skin allograft transplantation on chronic wounds and burns.

CONFLICT OF INTEREST
The authors declare no potential conflict of interest.

ORCID
Dominic Henn https://orcid.org/0000-0003-4775-0151

REFERENCES
1. Zaroff LI, Mills W Jr, Duckett JW Jr, Switzer WE, Moncrief JA. Multiple uses of viable cutaneous homografts in the burned patient. *Surgery*. 1966;59:368-372.

2. Cleland H, Wasiak J, Dobson H, et al. Clinical application and viability of cryopreserved cadaveric skin allografts in severe burn: a retrospective analysis. *Burns*. 2014;40:61-66.

3. Cuono CB, Langdon R, Birchall N, Barttelbort S, McGuire J. Composite autologous-allogeneic skin replacement: development and clinical application. *Plast Reconstr Surg*. 1987;80:626-637.

4. Franchini M, Zanini D, Bosinelli A, et al. Evaluation of cryopreserved donor skin viability: the experience of the regional tissue bank of Verona. *Blood Transfus*. 2009;7:100-105.

5. Mosti G, Mattaliano V, Magliaro A, Picerni P, Bastiani L. Cadaveric skin grafts may greatly increase the healing rate of recalcitrant ulcers when used both alone and in combination with split-thickness skin grafts. *Dermatol Surg*. 2019;46(2):169-179.

6. DiDomenico L, Landsman AR, Emch KJ, Landsman A. A prospective comparison of diabetic foot ulcers treated with either a cryopreserved skin allograft or a bioengineered skin substitute. *Wounds*. 2011;23:184-189.

7. Gurtner GC, Garcia AD, Bakewell K, Alarcon JB. A retrospective matched-cohort study of 3994 lower extremity wounds of multiple etiologies across 644 institutions comparing a bioactive human skin allograft, TheraSkin, plus standard of care, to standard of care alone. *Int Wound J*. 2019;17(1):55-64.

8. Towler MA, Rush EW, Richardson MK, Williams CL. Randomized, prospective, blinded-enrollment, head-to-head venous leg ulcer healing trial comparing living, bioengineered skin graft substitute (Apligraf) with living, cryopreserved, human skin allograft (TheraSkin). *Clin Podiatr Med Surg*. 2018;35:357-365.

9. Aggarwal SJ, Baxter CR, Diller KR. Cryopreservation of skin: an assessment of current clinical applicability. *J Burn Care Rehabil*. 1985;6:469-476.

10. Cinamon U, Eldad A, Chaouat M, et al. A simplified testing system to evaluate performance after transplantation of human skin preserved in glycerol or in liquid nitrogen. *J Burn Care Rehabil*. 1993;14:435-439.

11. Pirnay JP, Verween G, Pascual B, et al. Evaluation of a microbiological screening and acceptance procedure for cryopreserved skin allografts based on 14 day cultures. *Cell Tissue Bank*. 2012;13:287-295.

12. Garza RM, Press BH, Tyan DB, Karanas YL, Lee GK. Immunological effect of skin allograft in burn treatment: impact on future vascularized composite allotransplantation. *J Burn Care Res*. 2017;38:169-173.

13. Chen K, Vigliotti A, Bacca M, McMeeking RM, Deshpande VS, Holmes JW. Role of boundary conditions in determining cell alignment in response to stretch. *Proc Natl Acad Sci U S A*. 2018;115:986-991.

14. Fomovsky GM, Holmes JW. Evolution of scar structure, mechanics, and ventricular function after myocardial infarction in the rat. *Am J Physiol Heart Circ Physiol*. 2010;298:H221-H228.

15. Bredfeldt JS, Liu Y, Pehlke CA, et al. Computational segmentation of collagen fibers from second-harmonic generation images of breast cancer. *J Biomed Opt*. 2014;19:16007.

16. Odobasic D, Kitching AR, Holdsworth SR. Neutrophil-mediated regulation of innate and adaptive immunity: the role of myeloperoxidase. *J Immunol Res*. 2016;2016:2349817.

17. Bulloch K, Miller MM, Gal-Toth J, et al. CD11c/EYFP transgene illuminates a discrete network of dendritic cells within the embryonic, neonatal, adult, and injured mouse brain. *J Comp Neurol*. 2008;508:687-710.

18. Zhuang Q, Liu Q, Divito SJ, et al. Graft-infiltrating host dendritic cells play a key role in organ transplant rejection. *Nat Commun*. 2016;7:12623.

19. Nunez-Gutierrez H, Castro-Munozledo F, Kuri-Harcuch W. Combined use of allograft and autograft epidermal cultures in therapy of burns. *Plast Reconstr Surg*. 1996;98:929-939. discussion 940-921.

20. Yamamoto T, Iwase H, King TW, Hara H, Cooper DKC. Skin xenotransplantation: historical review and clinical potential. *Burns*. 2018;44:1738-1749.

21. Geer DJ, Swartz DD, Andreadis ST. In vivo model of wound healing based on transplanted tissue-engineered skin. *Tissue Eng*. 2004;10:1006-1017.

22. Padmanabhan J, Maan ZN, Kwon SH, Kosaraju R, Bonham CA, Gurtner GC. In vivo models for the study of fibrosis. *Adv Wound Care (New Rochelle)*. 2019;8:645-654.

23. Okazaki M, Fushida S, Harada S, et al. Establishing a xenograft mouse model of peritoneal dissemination of gastric cancer with organ invasion and fibrosis. *BMC Cancer*. 2017;17:23.

24. Morris AH, Chang J, Kyriakides TR. Inadequate processing of decellularized dermal matrix reduces cell viability in vitro and increases apoptosis and acute inflammation in vivo. *Biores Open Access*. 2016;5:177-187.

25. Lyons DA, Mendenhall SD, Neumeister MW, Cederna PS, Momoh AO. Aseptic versus sterile acellular dermal matrices in breast reconstruction: an updated review. *Plast Reconstr Surg Glob Open*. 2016;4:e823.

26. Li CL, Leng Y, Zhao B, et al. Human iPSC-MSC-derived xenografts modulate immune responses by inhibiting the cleavage of caspases. *Stem Cells*. 2017;35:1719-1732.

27. Benichou G, Yamada Y, Yun SH, Lin C, Fray M, Tocco G. Immune recognition and rejection of allogeneic skin grafts. *Immunotherapy*. 2011;3:757-770.

28. Etra JW, Grzelak MJ, Fidder SAJ, et al. A skin rejection grading system for vascularized composite allotransplantation in a preclinical large animal model. *Transplantation*. 2019;103:1385-1391.

29. Bruneau S, Woda CB, Daly KP, et al. Key features of the intragraft microenvironment that determine long-term survival following transplantation. *Front Immunol*. 2012;3:54.

30. Gurtner GC, Werner S, Barrandon Y, Longaker MT. Wound repair and regeneration. *Nature*. 2008;453:314-321.

31. Liu Y, Keikhosravi A, Mehta GS, Drifka CR, Eliceiri KW. Methods for quantifying fibrillar collagen alignment. *Methods Mol Biol*. 1627;2017:429-451.

32. Debeer S, Le Luduec JB, Kaiserlian D, et al. Comparative histology and immunohistochemistry of porcine versus human skin. *Eur J Dermatol*. 2013;23:456-466.